INSTITUTE OF PHYSICS PUBLISHING JOURNAL OF OPTICS A: PURE AND APPLIED OPTICS

J. Opt. A: Pure Appl. Opt. **5** (2003) 276–282 PII: S1464-4258(03)57310-X

Focusing evolution of generalized propagation invariant optical fields

J C Gutiérrez-Vega[1,3], **R Rodríguez-Masegosa**[1] **and S Chávez-Cerda**[2]

[1] Instituto Tecnológico y de Estudios Superiores de Monterrey, 64849 Monterrey NL, Mexico
[2] Instituto Nacional de Astrofísica, Optica y Electrónica, 72000 Puebla, Mexico

E-mail: juliocesar@itesm.mx

Received 30 November 2002, in final form 28 March 2003
Published 17 April 2003
Online at stacks.iop.org/JOptA/5/276

Abstract
The focusing evolution of apertured propagation invariant optical fields (PIOFs) with arbitrary transverse intensity distribution is analysed in detail. A decomposition of the PIOF into its constituent plane waves is applied to find a simple expression of the normalized intensity along the propagation axis which is valid for any PIOF. It is shown that the presence of an apparent focus close to the focal plane is a general property of any focused PIOF and that it is not related to the focal shift due to apertures. By selecting appropriate parameters it is possible to generate a second intense peak beyond the focal plane. Additionally, we define the conditions under which the original PIOF can be reconstructed beyond the focal plane with a desired magnification.

Keywords: Focusing, Bessel beams, non-diffracting beams, beam propagation

1. Introduction

The spatial evolution of propagation invariant optical fields (PIOFs) has been a subject of interest since it was shown by Durnin *et al* [1, 2] that such beams are diffraction-free mode solutions of the scalar wave equation. Since PIOFs are supposed to propagate in free homogeneous media they may be considered as a linear superposition of plane waves. The condition of invariant propagation requires that all constituent plane waves share a common phase velocity in the direction of propagation, say the z-axis. Consequently, they remain in phase and the wave preserves an invariant transverse structure under propagation. The plane wave expansion of an arbitrary monochromatic PIOF $U(x, y, z)$ is written in terms of the Whittaker solution [3] to the Helmholtz equation $\nabla^2 U + k^2 U = 0$ as

$$U(x, y, z \geqslant 0) = \exp(\mathrm{i}k_z z) \int_0^{2\pi} A(\varphi) \exp[\mathrm{i}k_t (x \cos\varphi + y \sin\varphi)] \, \mathrm{d}\varphi, \quad (1)$$

where $A(\varphi)$ is the continuous or discrete complex *annular* spectrum, $k_t = k \sin\theta_0$ and $k_z = k \cos\theta_0$ are the magnitudes of the transverse and longitudinal components of the wavevector $\boldsymbol{k}$ and temporal dependence $\exp(-\mathrm{i}\omega t)$ has been assumed, with ω being the light frequency. We have chosen to call the spectrum annular instead of the usual *angular* since, in fact, for any PIOF the set of wavevectors has the same angle $\theta_0 = \arccos(k_z/k)$ with respect to the propagation axis and their tips lie on an circular delta in the $\boldsymbol{k}$-space. This interpretation suggested the simplest experimental set-up, first introduced by Durnin *et al* [2] to generate a class of PIOFs, namely an annular ring modulated in magnitude and phase by a function (φ) and located at a focal distance of a convergent lens.

The function $A(\varphi)$ is the annular spectrum of the PIOF and defines the transverse structure of the field. It is well known [1, 2] that when $A(\varphi) = \exp(\mathrm{i}m\varphi)$, the invariant field corresponds to the mth-order Bessel beam $J_m(k_t r)\exp(\mathrm{i}m\varphi)$, which reduces to the fundamental mode J_0 when $m = 0$. The discrete case $A(\varphi) = \delta(\varphi - \pi/2) + \delta(\varphi + \pi/2)$ corresponds to a two-point Young experiment that produces a cosinoidal PIOF. Finally, an arbitrary complex function $A(\varphi)$ generates an arbitrary transverse distribution $U(x, y)$ which is still invariant under a propagation in z coordinate as follows immediately from equation (1) [4].

For most applications, the focusing properties of PIOFs are of crucial importance. For instance, recently Kullin *et al* [5]

[3] Author to whom any correspondence should be addressed.

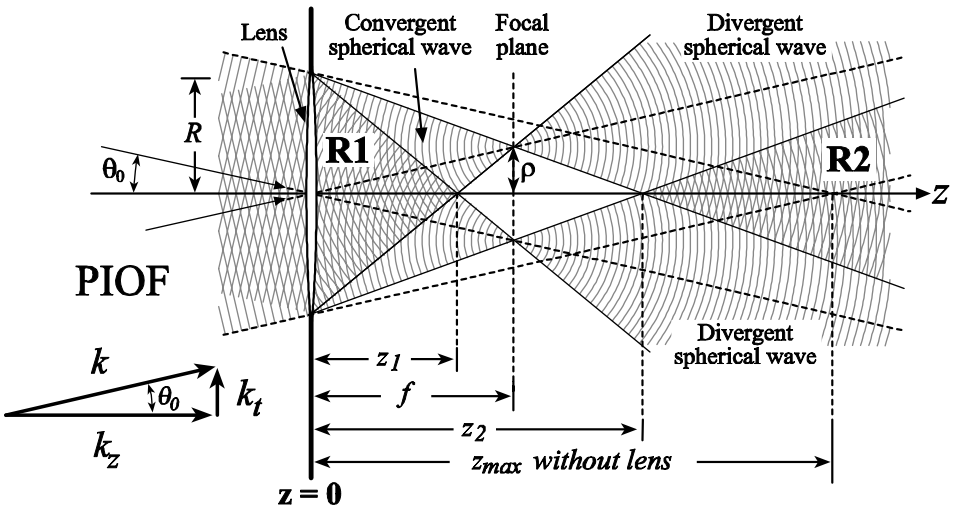

Figure 1. Geometrical evolution of the focusing of a PIOF.

used a focused Bessel beam to develop a single hollow-beam optical trap for cold atoms. For Bessel beams it is well known that the image in the Fraunhofer plane corresponds to a circular ring; however, the presence of an apparent focus ahead of the focal plane has been a subject of analysis and has often been related to the focal shift effect [6–9]. This effect has also been recognized to be present in focused apertured annular fields [10, 11], Bessel–Gauss beams [12, 13] and vector beams [14]. In general, the basic approach has consisted in solving the Fresnel diffraction integral in the region surrounding the focal plane of the lens using standard numerical techniques [8, 9, 15, 16]. In spite of the fact that many valuable and practical results have been found with this approach, it was demonstrated that the Fresnel diffraction integral could introduce slight errors in the diffraction of plane waves by apertures [17–20]. For Bessel beams, the existence of this pseudo-focus was explained in terms of the superposition of the constituent Hankel conical waves by Chávez-Cerda and New [21].

In this work, the focusing properties of apertured PIOFs with arbitrary intensity distribution are analysed in detail. In particular, we show that the presence of the apparent focus is not restricted to the Bessel beams, but is a general property of any focused PIOF. Our analysis reveals that, given a semiangle θ_0, the expression of the normalized intensity along the z-axis is the same for any focused PIOF with arbitrary transverse distribution; moreover, this expression is described with a simple relation involving only geometric parameters. By selecting appropriate parameters it is possible to generate a second intense peak beyond the focal plane. Additionally, we define the conditions under which the original PIOF can be reconstructed beyond the focal plane with a desired magnification. Throughout this work we use the term 'reconstruction' to mean the process when constituent plane waves interfere again beyond the focal plane and rebuild a second field with the same transverse shape as the original PIOF. Some simulations, that fully take into account diffraction effects, are included to corroborate our geometric-approximated formulae for the intensity along the z-axis. We compare these results with previous experimental observations [5]. This work consolidates and extends previous works on focused Bessel beams [6–9, 21].

2. Geometric optics of focused PIOFs

A schematic representation of the focal region of a PIOF is shown in figure 1. Consider that a PIOF characterized by an annular spectrum $A(\varphi)$ and semiangle θ_0 is impinging on a circular lens (radius R and focal length f) from the left. It is clear that the image formed in the focal plane is a thin ring properly modulated in amplitude and phase by $A(\varphi)$.

The behaviour of the focused PIOF outside the focal plane is better visualized if we concentrate our attention in the individual evolution of the constituent plane waves which form the PIOF. As we mentioned above, any PIOF can be expanded in a number of plane waves whose wavevectors lie on the surface of a cone defined by $\tan\theta_0 = k_t/k_z$.

Once the plane waves pass through the lens, they are transformed into converging spherical waves which interfere beyond the lens in the conical region labelled R1 in figure 1. It is straightforward to prove that the apex of region R1 is located at

$$z_1 = \frac{fR}{R+\rho}, \tag{2}$$

where

$$\rho = f\tan\theta_0$$

is the radius of the image ring where the spherical waves collapse. As the focal distance of the lens increases then z_1 increases; in the limit $f \to \infty$ the spherical waves become plane waves (i.e. the lens disappears) and the tip of R1 coincides with $z = z_{\max} = R/\tan\theta_0$. Beyond the focal plane the converging waves become diverging spherical waves; if the condition $\rho < R$ is satisfied then a second interfering conical region (R2) can be observed (see figure 1). Geometrically the tip of region R2 is located at

$$z_2 = \frac{fR}{R-\rho}. \tag{3}$$

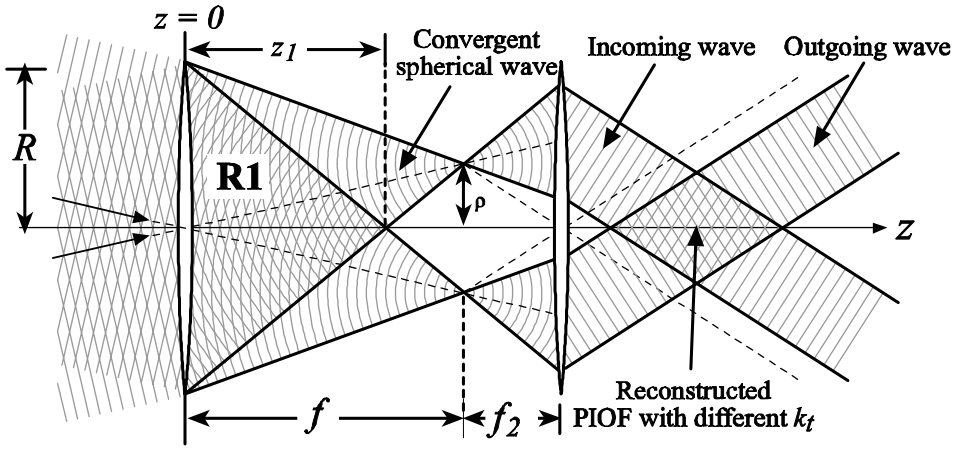

Figure 2. Geometrical evolution of the reconstruction of a focused PIOF when the second lens is located between the focal plane and the second peak at z_2. The incoming and outgoing waves superpose to build up together the original PIOF but with a different transverse wavenumber k_t.

Note that to assure the existence of the region R2 it is necessary that $\rho < R$, or equivalently, once the propagating semiangle θ_0 is defined, the existence of R2 is restricted to have $f < z_{\max}$. The superposition of spherical waves in R2 reproduces the original transverse distribution of the PIOF but now the pattern is expanding while it propagates. An invariant reconstruction of the original PIOF is achieved by considering the annular image in the focal plane as the input object of a second lens (L2) located beyond $z = f$. To have a successful invariant reconstruction it is a requisite that L2 collects the whole extent of the spherical wavefronts coming out from the image ring.

The reconstructed invariance region depends on the quantity of spherical wavefronts that the second lens collects. Evidently, if L2 is fully immersed in region R2 the invariance region will take the typical conical form similar to those created with the well known Durnin experiment [2]; however, if L2 is located just at z_2 the invariance region will take the form of a double cone similar to those created with an axicon; finally, when L2 is located between f and z_2 the reconstructed invariance region is as illustrated in figure 2.

The situation when the second lens is located at z_2 is interesting because the set-up could be employed to generate *incoming* waves from the original PIOF [21, 22] and extend its maximum propagation distance. This set-up has the advantage of using only lenses, which are more common in laboratories than axicons.

3. Axial intensity behaviour of focused PIOFs

The form of the intensity along the z-axis can be estimated by using geometrical arguments. Let us assume that the PIOF is composed by N plane waves. Beyond the lens, the plane waves become N converging spherical waves which collapse in the focal plane at N points located around a image ring of radius ρ (see figure 1). The positions of the image points are given by

$$\boldsymbol{r}_n = (\rho\cos\varphi_n, \rho\sin\varphi_n, f),$$

where $\varphi_n = 2\pi n/N$, $n = 0, 1, \ldots, N-1$. The three-dimensional field distribution U inside the geometrical cones

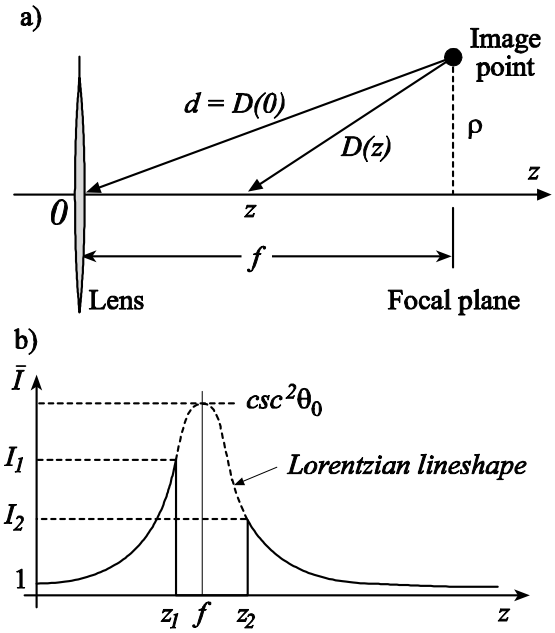

Figure 3. The geometric prediction of the axial intensity of a focused PIOF is given by a Lorentzian curve.

R1 and R2 results from the superposition of the N spherical waves, namely

$$U(\boldsymbol{r}) = \mathrm{e}^{\mathrm{i}kd}\sum_{n=0}^{N-1}\frac{A_n\exp(\mp\mathrm{i}k|\boldsymbol{r}-\boldsymbol{r}_n|)}{|\boldsymbol{r}-\boldsymbol{r}_n|}, \qquad (4)$$

where A_n are the complex amplitudes corresponding to the discrete annular spectrum $A(\varphi) = \Sigma A_n\delta(\varphi - \varphi_n)$. The negative and positive signs represent the converging and diverging behaviour of the spherical waves in the regions R1 and R2 respectively, the factor $|\boldsymbol{r}-\boldsymbol{r}_n|$ is the distance from the nth source point at $\boldsymbol{r}_n$ to the observation point at $\boldsymbol{r}$ and finally $d = |\boldsymbol{r}_n| = \sqrt{\rho^2 + f^2}$ is the distance from the image points to the origin (see figure 3(a)). Because of the circular symmetry of the ring, equation (4) can be simplified for points located along the z-axis. In particular, the separation between an axial

point at $\boldsymbol{r} = [0, 0, z]$ and the image points is given by

$$|\boldsymbol{r} - \boldsymbol{r}_n| = D(z) = \sqrt{\rho^2 + (z - f)^2}.$$

It follows that the terms involving the factor $|\boldsymbol{r} - \boldsymbol{r}_n|$ in equation (4) can be factored out of the summation, so the field along the z-axis reads

$$U(z) = \frac{\exp[\mp \mathrm{i}kD(z) + \mathrm{i}kd]}{D(z)} \sum_{n=0}^{N-1} A_n.$$

The summation of complex constants $\sum A_n$ is indeed another complex constant which can be written as $C\exp(\mathrm{i}\beta)$; consequently, the axial field $U(z)$ becomes

$$U(z) = \frac{C}{D(z)} \exp[\mp \mathrm{i}kD(z) + \mathrm{i}kd + \mathrm{i}\beta].$$

In this manner the intensity along the z-axis takes the form $I(z) = |U|^2 = (C/D)^2$, where the constant C is found by using the continuity of the known intensity at $z = 0$. If I_0 is the initial axial intensity of the PIOF and assuming a lossless lens then we find $C^2 = I_0 d^2 = I_0(\rho^2 + f^2)$, so the normalized axial intensity $\overline{I}(z) = I(z)/I_0$ can be written finally as follows.

For $z \in [0, z_1]$ and $z \in [z_2, \infty)$

$$\overline{I}(z) = \left[\frac{D(0)}{D(z)}\right]^2 = \frac{\rho^2 + f^2}{\rho^2 + (z - f)^2}, \tag{5}$$

and $\overline{I}(z) = 0$, for $z \in (z_1, z_2)$.

From a geometric point of view the normalized intensity along the z-axis is equal to the simple squared ratio between distances $D(0)$ and $D(z)$ (see figure 3(a)). Equation (5) defines a bell lineshape known as the *Lorentzian curve* centred at $z = f$ whose maximum value is $1 + (f/\rho)^2 = \mathrm{cosec}^2\,\theta_0$. A typical plot of the axial normalized intensity along the z-axis is shown in figure 3(b). Notice that $\overline{I}$ depends on the focal distance of the lens, and is always the same for any arbitrary PIOF with a given parameter θ_0. In particular, when f tends to infinity (i.e. the lens disappears) then $\overline{I} \to 1$ for $z \in [0, z_{\max}]$ and $\overline{I} = 0$ for $z \in (z_{\max}, \infty)$, as expected for an apertured PIOF.

The consequence of changing the radius of the circular lens on the axial intensity consists in modifying the position of the vertexes z_1 and z_2. In figure 1 we can observe that z_1 is closer to f than z_2 for any combination of values; specifically, we have

$$\frac{z_2 - f}{f - z_1} = \frac{R + \rho}{R - \rho} > 1.$$

This result implies that the first peak I_1 is always larger than the second peak I_2 (see figure 3(b)). The ratio between both peak intensities is found by substituting z_1 and z_2 in equation (5), namely

$$\frac{I_1}{I_2} = \frac{\rho^2 + (z_2 - f)^2}{\rho^2 + (z_1 - f)^2} > 1.$$

If the angle θ_0 of the PIOF decreases, then ρ decreases and z_1 and z_2 get closer to the focal plane; consequently, the peak intensities increase such that $I_2 \to I_1$. The limiting case occurs when $\theta_0 = 0$ (i.e. a plane wave normally incident into the lens) and both peaks coincide in the geometric focal point with an infinite intensity, i.e. $\mathrm{cosec}\,\theta_0 \to \infty$ as $\theta_0 \to 0$. For practical cases it is usual that $\rho \ll f$ and $R \ll f$ (it follows that $|z - f| \gg \rho$); consequently, the axial intensity equation (5) can be simplified to

$$\overline{I}(z) \simeq \frac{f^2}{(z - f)^2}, \tag{6}$$

for $z \in [0, z_1]$ and $z \in [z_2, \infty)$. Equation (5) has been deduced by using a PIOF with a discrete ring spectrum; however, an equivalent proof using integrals instead of summations can be carried out to validate that equation (5) also describes the axial intensity of a PIOF with a continuous annular spectrum. Specifically, when the spectrum $A(\varphi)$ is continuous, the summation $\sum A_n$ becomes the integral $\int_0^{2\pi} A(\varphi)\,\mathrm{d}\varphi$ whose result is indeed a complex number which can be written again as $C\exp(\mathrm{i}\beta)$. The integral is scaled out to satisfy that C could be determined by continuity of the intensity at $z = 0$. As an example, consider the annular spectrum of the higher-order Bessel beams $A(\varphi) = \exp(\mathrm{i}m\varphi)$. Since the integral $\int_0^{2\pi} \exp(\mathrm{i}m\varphi)\,\mathrm{d}\varphi$ vanishes, except for the lowest-order Bessel beam with $m = 0$, it implies that the axial intensity of the higher-order Bessel beams must be equal to zero.

4. Numerical evolution

Real focusing of PIOFs is evidently affected by the wave behaviour of the fields and the edge-diffracted waves produced by the lens. In order to confirm the validity of equation (5) for any PIOF, we simulate the focusing evolution of a cosinoidal PIOF and an arbitrary complex PIOF. Our numerical study is based on the numerical solution of the paraxial wave equation applying standard Fourier propagation methods [17, 23]. Plots of the focusing and the reconstruction of Bessel beams can be found in [5, 21].

4.1. Focusing of a cosinoidal PIOF

Suppose that a cosinoidal PIOF $U_t = \cos(k_t y)$ is normally incident on a circular lens with radius $R = 4$ mm and focal distance $f = 0.75$ m. We choose a value of the transverse propagation constant $k_t = 13\,238.895\ \mathrm{m}^{-1}$ to assure an image ring with radius $\rho = 1$ mm. The propagation of the focused cosinoidal field along the plane $(y$–$z)$ is displayed in figure 4. By comparing this wave evolution with respect to the geometric prediction sketched in figure 1, we can identify clearly the convergent and divergent spherical waves and the conical regions R1 and R2. As expected, the field in the focal plane is formed by two brilliant points at $(x, y) = (0, \pm\rho)$.

Inside the conical region R1 the converging spherical waves interfere, giving us the impression that the cosinoidal pattern is collapsing toward the geometric vertex located at $z_1 = 0.6$ m. Beyond $z_2 = 1$ m there exist the second conical region R2 where the cosinoidal-like field is reconstructed again. In figure 5 we show the intensity evolution in the region near the focal plane. Observe that the edge waves interfere constructively in the central region of the converging spherical waves, and that they propagate beyond the focal plane. Since the whole energy of the input field concentrates only in two points in the focal plane, it is expected that the intensity of the image peaks would be greater than the intensity I_1 at the

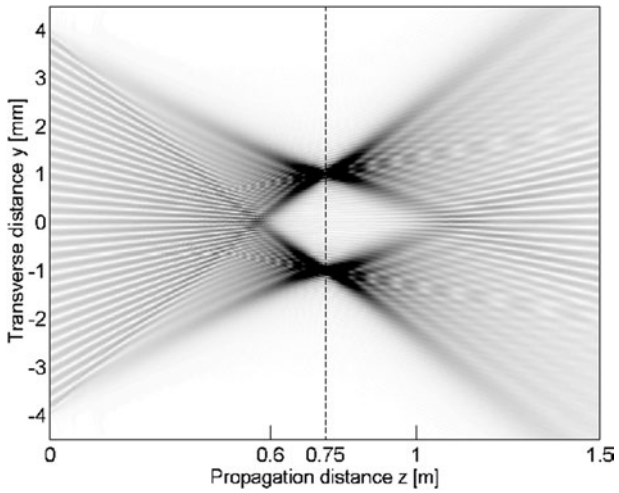

Figure 4. Evolution of the focusing of a cosinoidal field. Geometric parameters: $f = 0.75$ m, $R = 4$ mm. Input field parameters: $\lambda = 632.8$ nm, $k_t = 13\,238.895$ m^{-1}. Focused field values: $\rho_0 = 1$ mm, $z_1 = 0.6$ m, $z_2 = 1$ m.

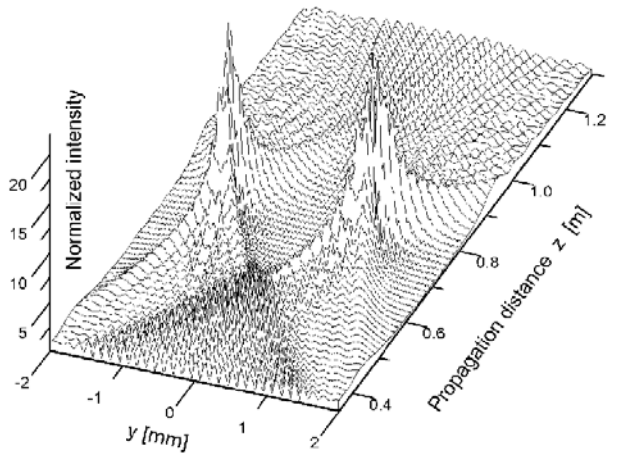

Figure 5. Evolution of a focused cosinoidal field in the region surrounding the focal plane.

first vertex. This effect is in contrast to the case of the Bessel beams; for them, the energy is uniformly distributed along the image ring, therefore I_1 becomes larger than the intensity in the ring. This fact would explain the tendency to consider the point located at z_1 as a focus of a Bessel beam [21].

In contrast to Bessel beams which have a peaked beam transverse distribution, the cosinoidal pattern presents fringes with the same intensity, that makes the 3D visualization of the axial intensity in figure 5 difficult; however, we show in figure 6(a) the behaviour of the normalized axial intensity for the cosinoidal field. By neglecting the diffractive fluctuations due to the edge waves, a very good agreement is observed with the geometrical evolution shown in dashed lines. Physical parameters are such that the second peak is not sufficiently high to be well defined; however, by decreasing the angle θ_0 of the PIOF we make z_1 and z_2 closer to the focal plane, so the second part of the plot tends to the geometrical prediction.

To confirm the last hypothesis we have simulated the focused evolution of a lowest-order Bessel beam $U_t = J_0(k_t\rho)$ with the same experimental parameters of the cosinoidal field

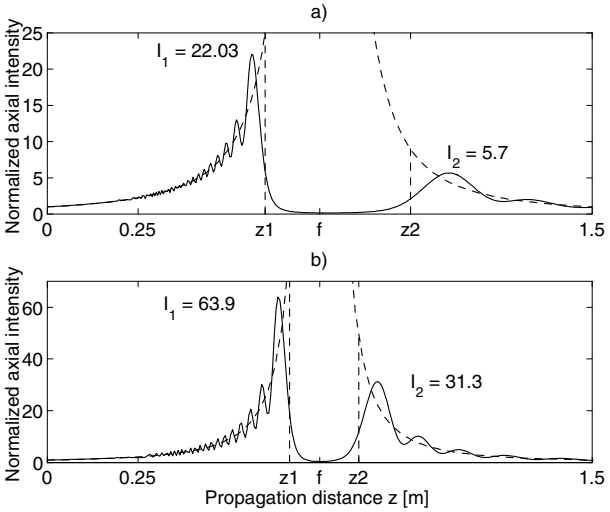

Figure 6. Evolution of the axial intensity of a focused cosinoidal field. The dashed lines represent the geometrical prediction.

simulation, but now the transverse spatial frequency k_t has been reduced to have an imaged ring with radius $\rho = 0.5$ mm. The new geometric vertices are located at $z_1 = 0.666$ m, and $z_2 = 0.857$ m. The normalized axial intensity is shown in figure 6(b) where a better defined second peak is observed. Since the image radius is small compared with the focal distance then a change of ρ does not affect significantly the Lorentzian curve displayed in figure 6(a). In this manner the most important consequence of changing ρ is to get the vertices closer each other. Furthermore, the existence of a second intense peak beyond the focal plane also is a general characteristic of the focusing of any PIOF.

Now we simulate the reconstruction process. Let us put a second lens (L2) between the focal plane and the second peak in the evolution displayed in figure 4. The lens L2 has a focal distance $f_2 = 0.2$ m and is placed at $z = 0.9$ m. The lens collects the divergent spherical waves emerging from the image points and transforms them into plane waves which interfere to form a second invariance region, see the geometrical prediction in figure 2. The results of simulating this situation are shown in figures 7 and 8. On the right-hand side of figure 8 we notice that the axial intensity of the reconstruction is about 25 times the axial intensity of the original PIOF. This magnification happens because the transverse extent of the reconstructed PIOF is smaller than the original PIOF, and evidently does not represent a violation of the conservation of energy. The effects of edge waves generated by L2 are clearly noted in both figures. As we commented above the reconstructed invariance region is maximized by placing the second lens farther away; in fact, the best results are obtained when it is completely immersed in region R2.

4.2. Focusing of a speckle-like PIOF

We now focus an arbitrary complex PIOF generated by the superposition of 20 plane waves with random complex amplitudes $|A_n| \leqslant 1$ and wavevectors randomly lying in a cone. This initial random distribution (see figure 9) has the interesting property that the intensity at the origin is not the maximum intensity of the initial pattern, and

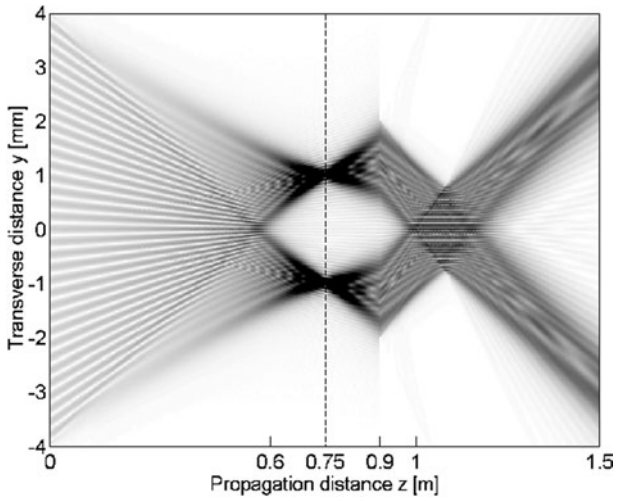

Figure 7. Evolution of the reconstruction of a focused cosinoidal field.

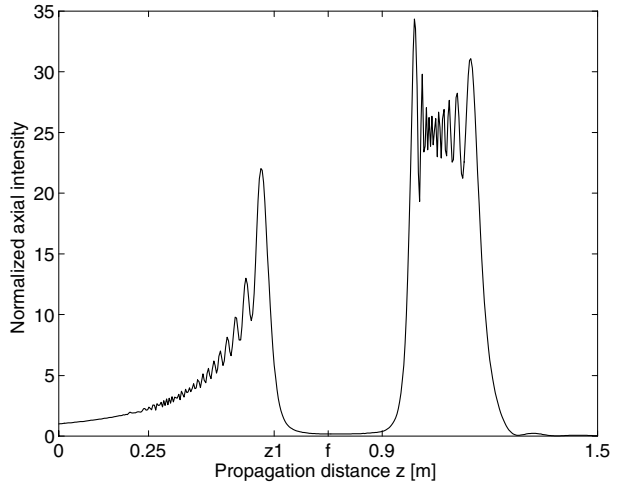

Figure 8. Axial normalized intensity of the focusing and the reconstruction of a cosinoidal field.

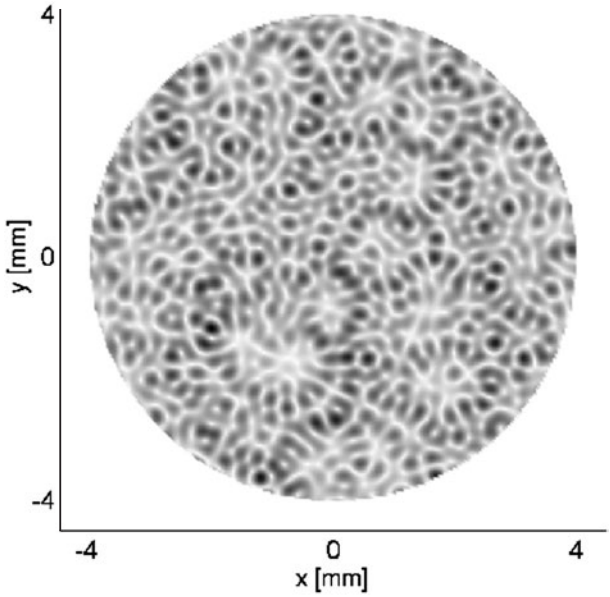

Figure 9. Transverse random intensity behind the lens.

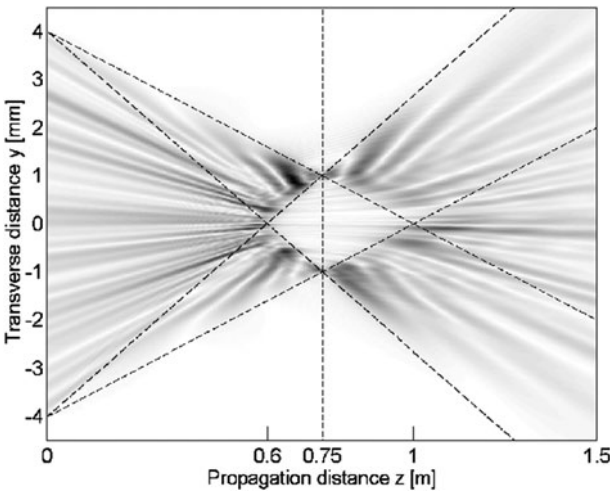

Figure 10. Evolution of the focusing of a random complex PIOF. Geometric parameters: $f = 0.75$ m, $R = 4$ mm. Input field parameters: $\lambda = 632.8$ nm, $k_t = 13\,238.895$ m^{-1}. Focused field values: $\rho_0 = 1$ mm, $z_1 = 0.6$ m, $z_2 = 1$ m.

moreover, it does not correspond to a local maximum of the intensity in the neighbourhood of the origin; however, it must still satisfy the behaviour predicted by equation (5). To make appropriate comparisons, we have preserved the same propagation parameters of the evolution of the cosinoidal pattern. The input field has been rescaled to have a unit intensity at the origin.

The propagation of the focused field along the plane (y–z) is shown in figure 10. Despite the randomness of the initial pattern, the evolution coincides with the geometric picture sketched in figure 1; however, now the conical limits of the regions R1 and R2 are not as evident as in figure 4. In contrast to the cosinoidal pattern, which focuses onto two points, the whole energy of this random pattern focuses onto 20 points, so it is expected that the ratio between the intensity of the imaged peaks and the intensity at z_1 would not be as well defined as in former case.

In figure 11 we display a zoom of the intensity in the plane (y–z) near the focal plane ($z = 0.75$ m). We can appreciate in the lens plane at $z = 0$ that the initial axial intensity does not correspond to a local maximum intensity around the z-axis. When the field is collapsing toward the focal plane, the axial intensity increases and it is high enough to guarantee the visualization of the intensity peak near z_1. The existence of the second region R2 behind the focal plane is revealed by the formation of the oscillating fringes. Observe that the converging field forms several intensity peaks outside the z-axis; in fact, some of them have a higher intensity than the peak located at z_1.

Figure 11 is interesting because it clearly demonstrates that the presence of the apparent focus at z_1 is only a consequence of the conical propagation of the constituent spherical waves of any focused PIOF. In fact, with this example we have shown that it is possible to generate other peaks with higher intensity than the intensity at the axial line. If the PIOF has a dominant maximum intensity at the origin (i.e. a beamlike profile) it is evident that the intensity peak at z_1 will be greater

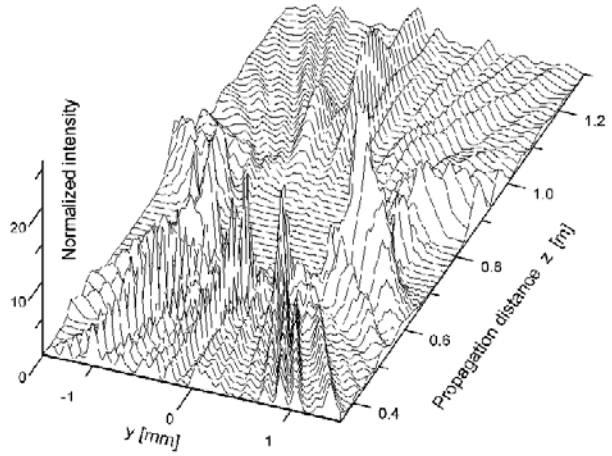

Figure 11. The evolution of a focused random complex PIOF in the region surrounding the focal plane.

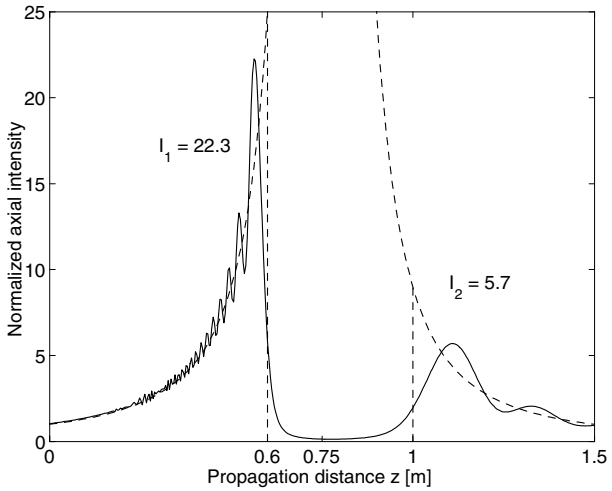

Figure 12. Evolution of the axial intensity of a focused random complex PIOF. Dashed lines represent the geometrical prediction.

than any peak formed outside the z-axis. Furthermore, if the PIOF is azimuthally symmetric (e.g. a Bessel beam) only the central peak is produced [21].

Finally, in figure 12 we show the evolution of the axial intensity for the speckle-like PIOF. Notice the similarity of this curve with respect to the evolution of the axial intensity for the cosinoidal PIOF shown in figure 6(a). After comparing both curves, we conclude that the transverse shape of the original PIOF does not affect the normalized axial intensity of the focused field, thus equation (5) is a good approximation to characterize the axial intensity of an arbitrary focused PIOF.

5. Conclusions

A detailed analysis of the focusing properties of apertured PIOFs with arbitrary transverse distribution has been presented. The decomposition of the PIOF into its constituent plane waves provides a useful geometric framework to visualize the evolution of the focused field and its reconstruction. The analysis reveals that the normalized intensity $\overline{I}$ along the z-axis can be described with a simple relation (equation (5)) involving only geometric parameters.

We have shown that the presence of the apparent focus close to the focal plane is a general property of any focused PIOF. Since this intense peak is simply a consequence of the conical symmetry of the constituent plane waves of the PIOF, it is not a geometric focus and it is not related to the so-called focal shift suffered by other apertured optical fields [6–9, 15, 16]. By adjusting the parameters it is possible to have a second intense peak beyond the focal plane (see figure 6(b)). Beyond this second point there exists a second conical region where the original PIOF is reconstructed. We have also shown that, given a semiangle θ_0, the expression of the normalized intensity along the z-axis is the same for any focused PIOF with arbitrary transverse distribution.

Acknowledgments

We acknowledge financial support from CONACyT México (grant no I-36456), and from the ITESM Research Chair in Optics (grant no CAT-007).

References

[1] Durnin J 1987 *J. Opt. Soc. Am.* A **4** 651–4
[2] Durnin J, Micely J J and Eberly J H 1987 *Phys. Rev. Lett.* **58** 1499–501
[3] Stratton J A 1941 *Electromagnetic Theory* (New York: McGraw-Hill) ch 6
[4] Turunen J, Vasara A and Friberg A T 1991 *J. Opt. Soc. Am.* A **8** 282–9
[5] Kullin S, Aubin S, Christe S, Peker B, Rolston S L and Orozco L A 2001 *J. Opt. B: Quantum Semiclass. Opt.* **3** 353–7
[6] De Nicola S 1996 *Pure Appl. Opt.* **5** 827–31
[7] Bouchal Z, Wagner J and Olivik M 1995 *Opt. Eng.* **34** 1680–7
[8] Lü B, Huang W and Zhang B 1995 *Opt. Commun.* **119** 6–12
[9] Lü B, Huang W, Zhang B, Kong F and Zhai Q 1996 *Opt. Commun.* **131** 223–8
[10] Poon T C 1988 *Opt. Commun.* **65** 401–6
[11] Bhabu S L and Poon T C 1991 *J. Opt. (Paris)* **22** 185–91
[12] Lü B and Huang W 1996 *J. Mod. Opt.* **43** 509–15
[13] Palma C, Cincotti G, Guattari G and Santarsiero M 1996 *J. Mod. Opt.* **43** 2269–77
[14] Greene P L and Hall D G 1999 *Opt. Express* **10** 411–9
[15] Born M and Wolf E 1999 *Principles of Optics* (Cambridge: Cambridge University Press)
[16] Siegman A 1986 *Lasers* (Mill Valley, CA: University Science)
[17] Chávez-Cerda S, Meneses-Nava M A and Hickmann J M 2000 *Opt. Lett.* **25** 83–4
[18] Dubra A and Ferrari J A 1999 *Am. J. Phys.* **67** 87–92
[19] Forbes G W 1996 *J. Opt. Soc. Am.* A **13** 1816–26
[20] Sheppard C J R 1992 *J. Opt. Soc. Am.* A **9** 274–81
[21] Chávez-Cerda S and New G H C 2000 *Opt. Commun.* **131** 369–78
[22] Chávez-Cerda S 1999 *J. Mod. Opt.* **46** 923–30
[23] Feit M D and Fleck J A 1988 *J. Opt. Soc. Am.* B **5** 633–40